

pubs.acs.org/NanoLett Letter

Confinement-Dependent Diffusiophoretic Transport of Nanoparticles in Collagen Hydrogels

Viet Sang Doan, SungGyu Chun, Jie Feng, and Sangwoo Shin*



Cite This: Nano Lett. 2021, 21, 7625-7630



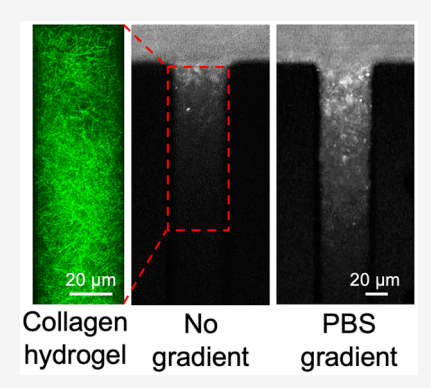
ACCESS I

Metrics & More

Article Recommendations

Supporting Information

ABSTRACT: The transport of nanoparticles in biological hydrogels is often hindered by the strong confinement of the media, thus limiting important applications such as drug delivery and disinfection. Here, we investigate nanoparticle transport in collagen hydrogels driven by diffusiophoresis. Contrary to common expectations for boundary confinement effects where the confinement hinders diffusiophoresis, we observe a nonmonotonic behavior in which maximum diffusiophoretic mobility is observed at intermediate confinement. We find that such behavior is a consequence of the interplay between multiple size-dependent effects. Our results display the utility of diffusiophoresis for enhanced nanoparticle transport in physiologically relevant conditions under tight confinement, suggesting a potential strategy for drug delivery in compressed tissues.



KEYWORDS: Nanoparticles, biohydrogel, diffusiophoresis, hindered transport

B iohydrogels, such as mucus and collagen gels, present a substantial barrier to the transport of solutes, macromolecules, and nanoparticles (NPs) due to the tight and tortuous geometry, enabling a number of important biological processes.1 For example, mucus limits the penetration of pathogens to protect the respiratory system.² In the extracellular matrix (ECM), the collagen network can act as a barrier to block tumor cell invasion.³ Extracellular space also determines the diffusion of neuroactive molecules in the brain, providing the ability to dispatch them in specific locations. 4 On the other hand, hindered transport in biohydrogels may also cause adverse effects. In bacterial biofilms, where bacteria live as a community within extracellular polymers, the hydrogel network serves as a shield against antibiotics, disinfectants, and detergents.⁵ ECM scaffolds hinder the delivery of oxygen and nutrient to the cell.⁶ In nanomedicine, the ECM significantly reduces the delivery efficiency of drug NPs, particularly in tumors and lungs. In this regard, the ability to control and enhance the NP transport in biohydrogels may offer new opportunities for a range of critical biological and biomedical systems.

Diffusiophoresis, which describes the directed migration of a colloidal or soluble species due to the concentration gradients of another species, is recognized as an effective mechanism for boosting the transport of microscale colloidal particles with aid of fast diffusion of molecular solutes. As solute gradients often arise within the biohydrogels that are present in various tissues, diffusiophoresis can be a potential strategy for enhancing the transport of NPs therein. The diffusiophoretic mobility defines the effectiveness of the particle diffusiopho-

resis for a given particle-solute pair, and the most commonly used expression for an electrolytic system is the classical size-independent mobility first pioneered by Deryaguin et al. ¹³ and then later formally derived by Prieve and Anderson. ^{14,15} In the limit of infinitesimally thin Debye layer (i.e., $\kappa a \to \infty$, where κ^{-1} is the Debye layer thickness and a is the particle radius), the diffusiophoretic mobility of a charged spherical particle immersed in a symmetric z: z electrolyte is given as

$$\mathcal{M}_{d0} = \frac{4\epsilon}{\mu} \left(\frac{k_{\rm B}T}{ze} \right)^2 (\beta \overline{\zeta} + \ln \cosh \overline{\zeta})$$
 (1)

where ϵ is the solution permittivity, μ is solution viscosity, $k_{\rm B}$ is the Boltzmann constant, T is the temperature, z is the valence, ϵ is the electron charge, $\overline{\zeta} = \frac{z\epsilon\zeta}{4k_{\rm B}T}$ is the dimensionless zeta potential, ζ is the particle zeta potential, and $\beta = (D_+ - D_-)/(D_+ + D_-)$ is the dimensionless diffusivity contrast between the cation (D_+) and the anion (D_-) .

Equation 1, which assumes the particle is in free space, has been widely used in a number of recent investigations. $^{16-27}$ Nevertheless, in many experimental studies, which almost always involve boundaries, the boundary effects on diffusio-

Received: June 10, 2021 Published: September 13, 2021





phoresis are commonly ignored by relying on the fact that diffusiophoresis exhibits reduced hydrodynamic interaction due to force-free migration, ⁸ despite no rigorous experimental investigation being made. This article aims to provide deeper insight into the boundary interactions of colloid diffusiophoresis by investigating the diffusiophoretic transport of NPs in tight porous hydrogels and suggest potential stategies to enhance drug delivery in compressed tissues.

To quantify the NP transport in porous media, we use a microfluidic setup in which an array of long, slender dead-end pores are selectively filled with collagen type I hydrogels (Figure 1a). To establish solute gradients across the hydrogels,

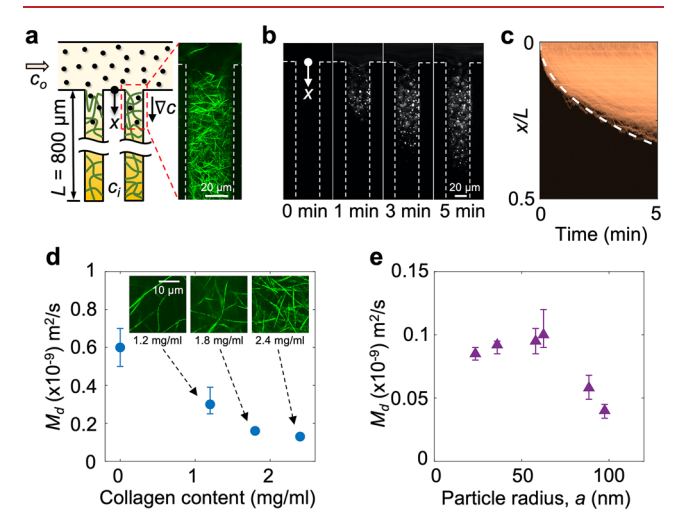


Figure 1. Confinement-dependent diffusiophoresis of nanoparticles (NPs) in collagen hydrogels. (a) A microfluidic platform to study NP diffusiophoresis in collagen hydrogels. The pores are filled with collagen type I. Inset is the collagen network selectively formed within the pore visualized by confocal reflectance microscopy. (b) aPS NPs (a = 100 nm) migrating into the collagen hydrogels (collagen concentration = 2.4 mg/mL) due to the solute gradient introduced by the sequential flow of inner solution (KAc, $c_i = 1 \text{ mM}$) followed by outer solution (KAc, $c_0 = 0.025 \,\mathrm{mM}$). (c) Spatiotemporal plot of fluorescence signal from (b). White curve is the theoretical prediction of the particle front to extract the diffusiophoretic mobility \mathcal{M}_d (see Supporting Information for details). (d) \mathcal{M}_d of aPS NPs (radius a =100 nm) versus collagen content. $c_i = 1$ mM; $c_o = 0.025$ mM KAc. Insets are the confocal images of collagen matrix at different concentrations. (e) \mathcal{M}_d of PS-PEG NPs versus the particle radius in collagen matrix (2.4 mg/mL). The particle radius varies from 24 to 98 nm. $c_i = 150$ mM; $c_o = 15$ mM NaCl.

we initially saturate the collagen hydrogels with a solution of solute concentration c_0 , followed by injecting another solution with concentration c_0 through the flow channel that runs over the hydrogel-filled pores. Particles suspended in the outer solution hence experience diffusiophoresis and migrate into the hydrogel (Figure 1b). By tracking the particle front over time, we can directly extract the diffusiophoretic mobility (Figure 1c, see Supporting Information for details). We neglect diffusioosmotic slip flow in our system due to the collagen fibrils having zero net charge near neutral pH.²⁸

We control the degree of boundary confinement effects on NP diffusiophoresis by varying either the pore (mesh) size or the particle size. We vary the collagen concentrations from 1.2 to 2.4 mg/mL to create hydrogels with various mesh sizes. We first measure the diffusiophoretic mobility of amine-functionalized polystyrene (aPS; $\zeta = +60 \text{ mV}$) NPs with a fixed radius

of a=100 nm under varying collagen concentrations. We impose a concentration gradient of potassium acetate (KAc; $c_0=0.025$ mM, $c_i=1$ mM; pH = 7.4) across the collagen hydrogel, where the solute concentration was chosen such that the NPs exhibit negligible adhesion to the collagen fibrils. As shown in Figure 1d, the diffusiophoretic mobility of aPS NPs gradually decreases as the collagen concentration is increased. Since the mesh size becomes smaller with increasing collagen concentration (mesh radius ~464 nm at 1.2 mg/mL to 267 nm at 2.4 mg/mL of collagen concentration; will be discussed later in detail), the resulting boundary confinement effect suppresses the particle motion, leading to reduced mobility.⁸

We also control the degree of confinement by changing the particle size while keeping the collagen concentration fixed. For this purpose, polystyrene-b-polyethylene glycol (PS-PEG; ζ = -21 mV) NPs are prepared via flash nanoprecipitation, 29,30 which enables easy synthesis of uniform NPs with controllable size (polydispersity index ~0.1). We use PS-PEG NPs with radii ranging from 24 to 98 nm, and sodium chloride (NaCl) for the solutes ($c_0 = 15 \text{ mM}$, $c_i = 150 \text{ mM}$; pH = 6.0). The collagen concentration is maintained at 2.4 mg/mL (mesh radius ≈267 nm). As we measure the mobility of PS-PEG NPs, we observe a nonmonotonic behavior in which the mobility exhibits a local maximum, displaying a stark contrast to the monotonic mobility of aPS NPs with fixed particle radius under varying mesh size. As shown in Figure 1e, the mobility increases with the particle radius up to a = 63 nm followed by a sudden decrease for larger particles.

Since the particle size is changed while the mesh size is kept constant, the nonmonotonic behavior of PS-PEG NPs is likely to be attributed to the two well-known size effects; the finite Debye layer and the boundary confinement effects. The finite Debye layer effect suppresses the phoretic motion because the driving force (solute gradient) is no longer tangential to the particle surface within the Debye layer, 15,31 which is likely to occur in NPs suspended in a dilute solution. 21,32,33 Also, the boundary effect generally suppresses the phoretic motion due to the increased hydrodynamic interactions, though it is believed to be less significant (i.e., $\sim 1/r^3$ flow field decay, where r is the distance away from the particle) than a particle dragged by a body force $(\sim 1/r \text{ decay})$. In the limit of small particle size where the confinement effect becomes negligible, the particle essentially experiences only the finite Debye layer effect, thus causing the mobility to increase with the particle radius. In the other limit where the particle is large, the boundary confinement effect becomes more prominent such that the phoretic motion is hindered as the particle becomes larger. Therefore, the nonmonotonic mobility is a consequence of the transition between the finite Debye layer effect and the boundary confinement effect.

While there is no analytical solution describing the particle diffusiophoresis accounting for both the finite Debye layer and the boundary confinement effects, Zydney developed a mathematical expression for electrophoresis of a weakly charged particle confined in a spherical cavity of radius h at arbitrary λ_1 and λ_2 , where $\lambda_1 = \kappa a$ and $\lambda_2 = a/h$ represent the dimensionless parameters for, respectively, the Debye layer and the boundary confinement effects. The spherical cavity may also represent a pore space formed in random fibrous media. The size-dependent electrophoretic mobility reads

$$\mathcal{M}_{e}(\lambda_{1}, \lambda_{2}) = \frac{\epsilon \zeta}{\mu} \left[\mathcal{A} - \mathcal{B} \left(\frac{1 - \lambda_{2}^{2}}{1 - \lambda_{2}^{5}} \right) \right]$$
 (2)

where \mathcal{A} and \mathcal{B} are both functions of λ_1 and λ_2 that need to be solved numerically (see Supporting Information).

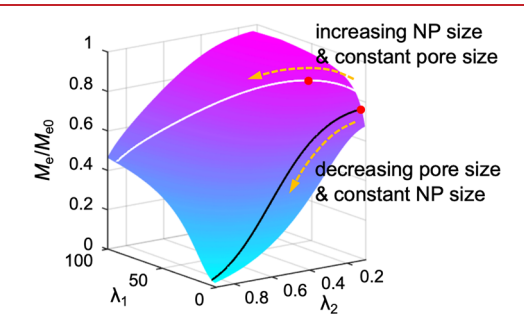


Figure 2. Size-dependent electrophoretic mobility. Electrophoretic mobility normalized by the Smoluchowski mobility $(\mathcal{M}_e/\mathcal{M}_{e0})$ by solving eq 2. Black curve represents mobility at $\lambda_1=4.2$, corresponding to the experimental conditions of aPS NPs (a=100 nm) in Figure 1d, and the white curve represents mobility at $\lambda_1=196\lambda_2$, corresponding to the experimental conditions of PS-PEG NPs in Figure 1e. Red dots indicate local maxima.

As shown in Figure 2, which plots eq 2 (normalized by the Smoluchowski mobility, $\mathcal{M}_{e0} = \epsilon \zeta / \eta$), the model qualitatively captures the mobility reduction due to both the Debye layer and the boundary confinement effects. For a varying pore size with a fixed particle radius, as is the case for aPS NPs, the mobility hindrance by boundary confinement effect becomes more significant as λ_2 becomes smaller (e.g., black curve in Figure 2 is when $\lambda_1 = 4.2$, corresponding to the experimental conditions for aPS NPs in Figure 1d). Also, the mobility hindrance becomes more dramatic as λ_1 decreases since the Debye layer extends across the entire cavity, so that the hydrodynamics around the particle exhibits 1/r decay. For the case where the particle size varies while other conditions are fixed, such as the pore radius h and the Debye layer thickness κ^{-1} , λ_1 and λ_2 both change simultaneously. This results in a nonmonotonic behavior in which the mobility shows a local maximum (e.g., white curve in Figure 2 is when $\lambda_1 = 196\lambda_2$ corresponding to the experimental conditions for PS-PEG NPs in Figure 1e).

Although this model only describes electrophoresis via an externally imposed electric field, the boundary effect on diffusiophoresis is expected to be similar to electrophoresis due to their associated hydrodynamics being identical. In this regard, we attempt to compare this model with the experimental results. As eq 2 considers the phoretic motion of a particle in a unit cavity, a fair comparison can only be made by accounting for the steric effect that arises in tortuous porous media since the experimental data shown in Figures 1d,e represent particle migration across many random pores.

Similar to hindered diffusion,³⁵ the steric effect can be addressed by introducing the steric factor S, which depends on the particle and pore geometry. Johansson and Löfroth obtained S for polymeric hydrogels via Brownian dynamics simulations, given as³⁶

$$S = \exp(-0.84f^{1.09}) \tag{3}$$

where $f=(1+a/t)^2\phi$ is the adjusted volume fraction of polymers, ϕ is the volume fraction, and t is the polymer (fibril) radius (~162 nm for collagen type I³⁷). The polymer volume fraction ϕ can be evaluated from the Darcy permeability k, for which we determine from previously reported experimental data for collagen type I hydrogels.^{7,38} Using k and ϕ , we also estimate the effective pore radius h by solving the Kozeny–Carman equation, which varies from h=464 nm at 1.2 mg/mL to 267 nm at 2.4 mg/mL of collagen concentration (see Supporting Information for details).

We verify eq 3 experimentally by measuring the hindered diffusivity, that is, reduction in the particle diffusivity in porous media (D) relative to that in free space (D_0) . The hindered diffusion in porous hydrogels is a consequence of not just the steric effect but also the hydrodynamic effect; thus the diffusivity hindrance can be expressed as the product of the two effects^{35,39}

$$\frac{D}{D_0} = \mathcal{F} \cdot \mathcal{S} \tag{4}$$

where $\mathcal F$ is a factor that takes into account the hydrodynamic interaction, which can be evaluated by solving the Brinkman equation as 35,40

$$\mathcal{F} = \left(1 + \frac{a}{k^{1/2}} + \frac{a^2}{9k}\right)^{-1} \tag{5}$$

We measure the diffusivity of dilute NPs either via single particle tracking or collective particle diffusion experiments depending on the particle size (see Supporting Information for details), where Figure 3 shows D/D_0 for various NPs in

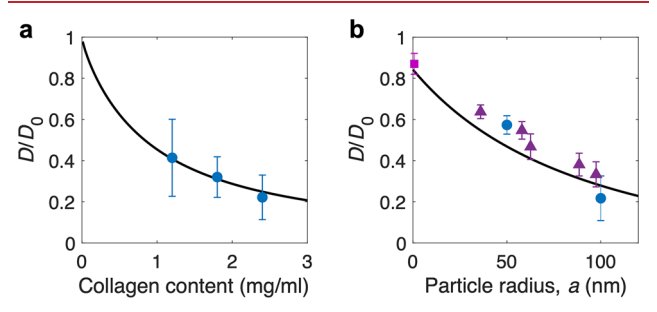


Figure 3. Hindered diffusion under confinement. Particle diffusivity in collagen hydrogels normalized by the free space diffusivity (D/D_0) with varying (a) collagen content and (b) particle radius. (a) D/D_0 versus collagen content for aPS NPs $(a=100~\rm nm)$. (b) D/D_0 versus particle radius in 2.4 mg/mL collagen matrix. Blue circles and purple triangles correspond to aPS and PS–PEG NPs, respectively. Magenta square represents a molecular dye (HPTS), where the radius $a=0.7~\rm nm$ is determined from the Stokes–Einstein relation. Black curves correspond to eqs $3-5~\rm cm$

collagen hydrogels. As expected, the diffusivity decreases either by increasing the particle size (Figure 3a) or the collagen content (Figure 3b), both of which increase the degree of confinement. The good agreement between the experimentally measured D/D_0 and eqs 3–5 (black curves in Figure 3) allows us to use eq 3 for $\mathcal S$ to account for the geometrical tortuosity of the measured diffusiophoresis, such that a direct comparison can be made between the experimental data and eq 2.

As shown in Figure 4, Zydney's model (black solid curves) agrees reasonably with the measured diffusiophoretic mobility rescaled by the steric factor, $(\mathcal{M}_d/\mathcal{M}_{d0})\cdot(1/\mathcal{S})$, though the

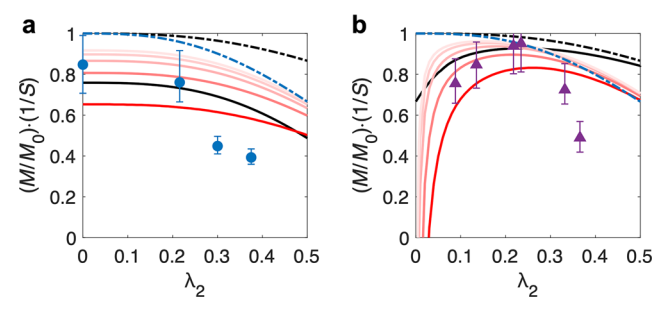


Figure 4. Hindered diffusiophoresis is a consequence of multiple size-dependent effects. Replotting of the data from Figures 1d,e by accounting for the steric factor S. Black solid curves represent (a) black ($\lambda_1 = 4.2$) and (b) white ($\lambda_1 = 196\lambda_2$) curves from Figure 2. Black dash-dot curves represent eq 2 at $\lambda_1 \to \infty$. Blue dash-dot curves represent particle mobility at an offset from the center of the cavity by half the distance from the particle surface to the cavity wall (data obtained from Table 1 of ref 40. Red curves represent particle mobility in the presence of Debye layer polarization (eq 6); (a) λ_1 varies from 20 to 100 (light to dark) with intervals of 20, (b) $\lambda_1 = p\lambda_2$ where p varies from 200 to 1000 (light to dark) with intervals of 200. For all the curves, S = 1.

model appears to be somewhat overpredicting the mobility, particularly at large λ_2 . As this model considers an idealized condition where the particle is assumed to be located exactly at the center of the spherical cavity, it does not reflect a realistic situation in which a particle will enter and leave the cavity at a random position and direction, thus representing an upper bound for the confinement effect. Therefore, relaxation of such an assumption must lead to more dramatic reduction in the mobility at a larger λ_2 .

A full numerical simulation by Lee and Keh indeed predicts that a small offset from the center of the cavity can lead to more pronounced confinement effect due to the increased hydrodynamic interaction. ⁴¹ Shown as blue dash-dot curves in Figure 4 (data taken from Table 1 of ref 40) for a particle with vanishing Debye layer $(\lambda_1 \to \infty)$, the mobility drops more rapidly at larger λ_2 compared to the ideal case (no offset; black dash-dot curves. This plots eq 2 in the limit of $\lambda_1 \to \infty$). For instance, when the center of a particle is offset from the center of the cavity by, say, half the distance from the particle surface to the cavity wall (i.e., 0.5(h-a)), then the mobility can drop by 35% from the free space mobility at $\lambda_2 = 0.5$ compared to only 13% drop in the absence of an offset, indicating the significant impact of particle position on diffusiophoresis in a confined space.

Another aspect that Zydney's model neglects is the asymmetric distortion of the Debye layer due to the advective ion transport within the Debye layer and/or due to the wall interaction, both of which lead to the polarization of the Debye layer that results in reduced phoretic motion. The polarization can be safely neglected only when $\exp\{2e|\zeta|/(k_{\rm B}T)\}/\lambda_1 \rightarrow 0$, which is clearly not the case in our experiments (e.g., 0.7 for aPS, and 0.02–0.09 for PS–PEG NPs) primarily due to the small λ_1 of NPs, making them highly susceptible to the polarization effect.

Recently, Chiu and Keh obtained a closed-form solution for the diffusiophoresis of weakly charged particles in a spherical cavity in the limit of relatively thin $(\lambda_1 > O(10))$ but polarizable Debye layer. ⁴⁴ The mobility reads

$$\mathcal{M}_{d} = \frac{2\epsilon}{\mu} \left(\frac{k_{B}T}{ze} \right)^{2} \left[\frac{5}{3} \left(\frac{1 + \lambda_{2} + \lambda_{2}^{2}}{1 + \lambda_{2} + \lambda_{2}^{2} + \lambda_{2}^{3} + \lambda_{2}^{4}} \right) - 1 \right] C$$
(6)

where C is a closed-form function of both λ_1 and λ_2 (see Supporting Information for the complete expression). Equation 6 (normalized by eq 1) is plotted as red solid curves in Figure 4 which shows that the theory successfully predicts more dramatic reduction in the mobility at large λ_2 as the Debye layer becomes thicker (decrease in λ_1). As anticipated, the polarization-induced hindrance becomes more pronounced at small λ_1 and large λ_2 , conditions for which the Debye layer deviates from the equilibrium structure in free space. While both models for offset and polarization effects presented in Figure 4 assume large λ_1 , which does not accurately render our system, we expect for both of these effects to strengthen as λ_1 is decreased. Since a thick Debye layer can amplify both effects, an even more rapid decrease in the mobility can be expected at small λ_1 , as we have observed experimentally.

The above findings also indicate that, provided that λ_1 is sufficiently large, diffusiophoresis can be an effective transport mechanism in strongly confined systems, which would otherwise be extremely difficult to achieve with diffusion or pressure-driven flows. A possible application of NP diffusiophoresis in such conditions is drug delivery in compressed tissues such as tumors. This would involve physiological conditions under which λ_1 is extremely large due to the high ionic strength of bodily fluids, and λ_2 is also large due to the high collagen content with additional components present in the extracellular matrix. Drug delivery to cancer cells requires an ample amount of chemotherapeutic NPs to migrate across the tight interstitium.^{7,45} However, due to the lack of interstitial flow, diffusion is believed to be the main transport mechanism for NPs inside the tumor microenvironment, resulting in a poor drug delivery efficiency. 46

As a proof of concept, we have tested the delivery of PS–PEG NPs (a=63 nm) under conditions relevant to the tumor interstitium. The collagen content is raised to 8 mg/mL (Figure 5a), creating a tight matrix ($\lambda_2 \approx 0.56$) that is initially filled with 1× phosphate buffer saline (PBS) solution ($\lambda_1 \approx 83$). As the polymeric PEG-coated NPs are widely used as drug delivery carriers,⁴⁷ such physiologically relevant conditions

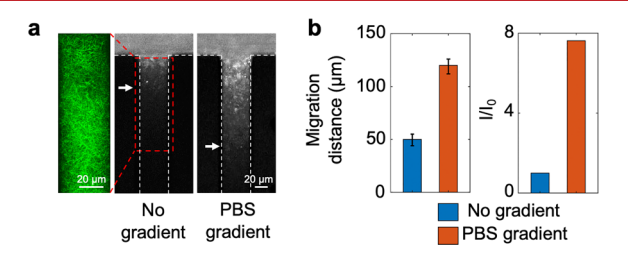


Figure 5. Enhanced diffusiophoretic delivery of NPs in concentrated collagen matrix under physiologically relevant conditions. (a) Migration of PS–PEG NPs ($a=63\,$ nm) via diffusion (middle panel) or diffusiophoresis (right panel) in concentration collagen matrix (left panel), which mimics physical conditions in solid tumor. The solute conditions for the diffusion experiment is $c_i=c_o=1\times$ PBS, and for diffusiophoresis is $c_i=1\times$ PBS, $c_o=0.01\times$ PBS + 298 mM glucose. The NP images were taken 10 min after the injection of the NP suspension. (b) Penetration distance at half-maximum intensity and the total intensity gain of PS–PEG NPs via diffusion (no gradient) and diffusiophoresis (PBS gradient).

mimic NP-oriented drug delivery into the tumor interstitium. 7,26

We measure the penetration distance and the total number of accumulated NPs in the collagen matrix over the course of 10 min. We compare diffusion and diffusiophoresis of PS-PEG NPs. Diffusion is established by maintaining the solute concentration at 1× PBS uniformly across the entire hydrogels, whereas diffusiophoresis is induced by injecting 0.01× PBS over 1× PBS filled hydrogels. For clinical feasibility, we supplement glucose to the injecting 0.01× PBS solution to maintain constant osmolarity at 0.3 Osm/L, which can help prevent critical side effects such as hypovolemia and hypotension.⁴⁸ The results in Figure 5b show that with the presence of PBS gradient, PS-PEG NPs migrate about 2.5 times further across the dense collagen matrix where the penetration distance is the location in the dead-end pore at half-maximum intensity. The fluorescence intensity gain I/I_0 within the dead-end pore, which reflects the improvement in the total number of penetrated particles compared to diffusion, shows nearly an 8-fold enhancement. These observations suggest diffusiophoresis as a potential strategy to enhance drug delivery efficiency under physiologically relevant conditions.

To summarize, we have investigated the boundary effects on NP diffusiophoresis in collagen hydrogels. We have shown that diffusiophoretic mobility of NPs can behave nonmonotonically under certain conditions, in which we observed both the increase and decrease in the mobility with varying particle size. These observations are attributed to the complex interplay between multiple size-dependent effects that are likely to arise in confined spaces. While we rationalized our results with several existing models that partially captures our observations to some degree, the lack of quantitative agreement warrants further studies in mathematical modeling of phoretic transport in complex microenvironments. Our results also highlight the use of diffusiophoresis as an effective transport mechanism under tight confinement when the ionic strength of the solution is high, suggesting the potential application of diffusiophoresis in nanomedicine.

ASSOCIATED CONTENT

Supporting Information

The Supporting Information is available free of charge at https://pubs.acs.org/doi/10.1021/acs.nanolett.1c02251.

Materials, experimental methods, and theoretical models of hindered diffusiophoresis in porous media (PDF)

AUTHOR INFORMATION

Corresponding Author

Sangwoo Shin — Department of Mechanical and Aerospace Engineering, University at Buffalo, The State University of New York, Buffalo, New York 14260, United States;
ocid.org/0000-0001-5618-8522; Email: sangwoos@buffalo.edu

Authors

Viet Sang Doan — Department of Mechanical and Aerospace Engineering, University at Buffalo, The State University of New York, Buffalo, New York 14260, United States SungGyu Chun — Department of Mechanical Science and Engineering, University of Illinois at Urbana—Champaign, Urbana, Illinois 61801, United States Jie Feng — Department of Mechanical Science and Engineering, University of Illinois at Urbana—Champaign, Urbana, Illinois 61801, United States; Materials Research Laboratory, University of Illinois at Urbana—Champaign, Urbana, Illinois 61801, United States; orcid.org/0000-0002-4891-9214

Complete contact information is available at: https://pubs.acs.org/10.1021/acs.nanolett.1c02251

Notes

The authors declare no competing financial interest.

ACKNOWLEDGMENTS

This material is based upon work supported by the National Science Foundation under Grant CBET-1930691.

REFERENCES

- (1) Masaro, L.; Zhu, X. X. Physical models of diffusion for polymer solutions, gels and solids. *Prog. Polym. Sci.* **1999**, 24, 731–775.
- (2) Zanin, M.; Baviskar, P.; Webster, R.; Webby, R. The interaction between respiratory pathogens and mucus. *Cell Host Microbe* **2016**, 19, 159–168.
- (3) Grossman, M.; Ben-Chetrit, N.; Zhuravlev, A.; Afik, R.; Bassat, E.; Solomonov, I.; Yarden, Y.; Sagi, I. Tumor cell invasion can be blocked by modulators of collagen fibril alignment that control assembly of the extracellular matrix. *Cancer Res.* **2016**, *76*, 4249–4258.
- (4) Syková, E.; Nicholson, C. Diffusion in brain extracellular space. *Physiol. Rev.* **2008**, *88*, 1277–1340.
- (5) Lieleg, O.; Ribbeck, K. Biological hydrogels as selective diffusion barriers. *Trends Cell Biol.* **2011**, 21, 543–551.
- (6) Axpe, E.; Chan, D.; Offeddu, G. S.; Chang, Y.; Merida, D.; Hernandez, H. L.; Appel, E. A. A multiscale model for solute diffusion in hydrogels. *Macromolecules* **2019**, *52*, 6889–6897.
- (7) Ramanujan, S.; Pluen, A.; McKee, T. D.; Brown, E. B.; Boucher, Y.; Jain, R. K. Diffusion and convection in collagen gels: implications for transport in the tumor interstitium. *Biophys. J.* **2002**, 83, 1650–1660
- (8) Anderson, J. L. Colloid transport by interfacial forces. *Annu. Rev. Fluid Mech.* **1989**, *21*, 61–99.
- (9) Velegol, D.; Garg, A.; Guha, R.; Kar, A.; Kumar, M. Origins of concentration gradients for diffusiophoresis. *Soft Matter* **2016**, *12*, 4686–4703.
- (10) Shin, S. Diffusiophoretic separation of colloids in microfluidic flows. *Phys. Fluids* **2020**, *32*, 101302.
- (11) Gerweck, L. E.; Seetharaman, K. Cellular pH gradient in tumor versus normal tissue: potential exploitation for the treatment of cancer. *Cancer Res.* **1996**, *56*, 1194–1198.
- (12) Allen, A.; Flemström, G. Gastroduodenal mucus bicarbonate barrier: protection against acid and pepsin. *Am. J. Physiol. Cell Physiol.* **2005**, 288, C1–C19.
- (13) Derjaguin, B. V.; Dukhin, S. S.; Korotkova, A. A. Diffusiophoresis in electrolyte solutions and its role in mechanism of film formation from rubber latexes by method of ionic deposition. *Kolloidn. Zh.* **1961**, *23*, *53*.
- (14) Anderson, J. L.; Prieve, D. C. Diffusiophoresis: Migration of Colloidal Particles in Gradients of Solute Concentration. *Sep. Purif. Methods* **1984**, *13*, 67–103.
- (15) Prieve, D. C.; Anderson, J. L.; Ebel, J. P.; Lowell, M. E. Motion of a particle generated by chemical gradients. Part 2. Electrolytes. *J. Fluid Mech.* **1984**, *148*, 247–269.
- (16) Abécassis, B.; Cottin-Bizonne, C.; Ybert, C.; Ajdari, A.; Bocquet, L. Boosting migration of large particles by solute contrasts. *Nat. Mater.* **2008**, *7*, 785–789.
- (17) Palacci, J.; Abecassis, B.; Cottin-Bizonne, C.; Ybert, C.; Bocquet, L. Colloidal motility and pattern formation under rectified diffusiophoresis. *Phys. Rev. Lett.* **2010**, *104*, 138302.

- (18) Yadav, V.; Freedman, J. D.; Grinstaff, M.; Sen, A. Bone-Crack Detection, Targeting, and Repair Using Ion Gradients. *Angew. Chem., Int. Ed.* **2013**, *52*, 10997–11001.
- (19) Kar, A.; Chiang, T.-Y.; Rivera, I. O.; Sen, A.; Velegol, D. Enhanced transport into and out of dead-end pores. *ACS Nano* **2015**, 9, 746–753.
- (20) Paustian, J. S.; Angulo, C. D.; Nery-Azevedo, R.; Shi, N.; Abdel-Fattah, A. I.; Squires, T. M. Direct measurements of colloidal solvophoresis under imposed solvent and solute gradients. *Langmuir* **2015**, *31*, 4402–4410.
- (21) Shin, S.; Um, E.; Sabass, B.; Ault, J. T.; Rahimi, M.; Warren, P. B.; Stone, H. A. Size-dependent control of colloid transport via solute gradients in dead-end channels. *Proc. Natl. Acad. Sci. U. S. A.* **2016**, 113, 257–261.
- (22) Shi, N.; Nery-Azevedo, R.; Abdel-Fattah, A. I.; Squires, T. M. Diffusiophoretic Focusing of Suspended Colloids. *Phys. Rev. Lett.* **2016**, *117*, 258001.
- (23) Shin, S.; Ault, J. T.; Feng, J.; Warren, P. B.; Stone, H. A. Lowcost zeta potentiometry using solute gradients. *Adv. Mater.* **2017**, 29, 1701516.
- (24) Nery-Azevedo, R.; Banerjee, A.; Squires, T. M. Diffusiophoresis in Ionic Surfactant Gradients. *Langmuir* **2017**, 33, 9694–9702.
- (25) Battat, S.; Ault, J. T.; Shin, S.; Khodaparast, S.; Stone, H. A. Particle entrainment in dead-end pores by diffusiophoresis. *Soft Matter* **2019**, *15*, 3879–3885.
- (26) Shin, S.; Doan, V. S.; Feng, J. Osmotic Delivery and Release of Lipid-Encapsulated Molecules via Sequential Solution Exchange. *Phys. Rev. Appl.* **2019**, *12*, 024014.
- (27) Doan, V. S.; Saingam, P.; Yan, T.; Shin, S. A Trace Amount of Surfactants Enables Diffusiophoretic Swimming of Bacteria. *ACS Nano* **2020**, *14*, 14219–14227.
- (28) Li, Y.; Asadi, A.; Monroe, M. R.; Douglas, E. P. pH effects on collagen fibrillogenesis in vitro: Electrostatic interactions and phosphate binding. *Mater. Sci. Eng., C* **2009**, *29*, 1643–1649.
- (29) Tian, C.; Feng, J.; Cho, H. J.; Datta, S. S.; Prud'homme, R. K. Adsorption and denaturation of structured polymeric nanoparticles at an interface. *Nano Lett.* **2018**, *18*, 4854–4860.
- (30) Tian, C.; Feng, J.; Prud'homme, R. K. Adsorption dynamics of polymeric nanoparticles at an air-water interface with addition of surfactants. *J. Colloid Interface Sci.* **2020**, *575*, 416.
- (31) Keh, H. J.; Wei, Y. K. Diffusiophoretic mobility of spherical particles at low potential and arbitrary double-layer thickness. *Langmuir* **2000**, *16*, 5289–5294.
- (32) Ha, D.; Seo, S.; Lee, K.; Kim, T. Dynamic Transport Control of Colloidal Particles by Repeatable Active Switching of Solute Gradients. ACS Nano 2019, 13, 12939–12948.
- (33) Shimokusu, T. J.; Maybruck, V. G.; Ault, J. T.; Shin, S. Colloid Separation by CO₂-Induced Diffusiophoresis. *Langmuir* **2020**, *36*, 7032–7038.
- (34) Zydney, A. L. Boundary effects on the electrophoretic motion of a charged particle in a spherical cavity. *J. Colloid Interface Sci.* **1995**, 169, 476–485
- (35) Phillips, R. J.; Deen, W. M.; Brady, J. F. Hindered transport of spherical macromolecules in fibrous membranes and gels. *AIChE J.* **1989**, 35, 1761–1769.
- (36) Johansson, L.; Löfroth, J.-E. Diffusion and interaction in gels and solutions. 4. Hard sphere Brownian dynamics simulations. *J. Chem. Phys.* **1993**, 98, 7471–7479.
- (37) Dutov, P.; Antipova, O.; Varma, S.; Orgel, J. P. R. O.; Schieber, J. D. Measurement of elastic modulus of collagen type I single fiber. *PLoS One* **2016**, *11*, No. e0145711.
- (38) Jackson, G. W.; James, D. F. The permeability of fibrous porous media. *Can. J. Chem. Eng.* **1986**, *64*, 364–374.
- (39) Johnson, E. M.; Berk, D. A.; Jain, R. K.; Deen, W. M. Hindered diffusion in agarose gels: test of effective medium model. *Biophys. J.* **1996**, 70, 1017–1023.
- (40) Solomentsev, Y. E.; Anderson, J. L. Rotation of a sphere in Brinkman fluids. *Phys. Fluids* **1996**, *8*, 1119–1121.

- (41) Lee, T. C.; Keh, H. J. Electrophoretic motion of a charged particle in a charged cavity. *Eur. J. Mech.* **2014**, *48*, 183–192.
- (42) O'Brien, R. W. The solution of the electrokinetic equations for colloidal particles with thin double layers. *J. Colloid Interface Sci.* **1983**, 92, 204–216.
- (43) Prieve, D. C.; Roman, R. Diffusiophoresis of a rigid sphere through a viscous electrolyte solution. *J. Chem. Soc., Faraday Trans.* 2 1987, 83, 1287–1306.
- (44) Chiu, H. C.; Keh, H. J. Electrophoresis and diffusiophoresis of a colloidal sphere with double-layer polarization in a concentric charged cavity. *Microfluid. Nanofluid.* **2017**, *21*, 45.
- (45) Zhao, Y.; Fay, F.; Hak, S.; Perez-Aguilar, J. M.; Sanchez-Gaytan, B. L.; Goode, B.; Duivenvoorden, R.; de Lange Davies, C.; Bjørkøy, A.; Weinstein, H.; Fayad, Z. A.; Perez-Medina, C.; Mulder, W. J. M. Augmenting drug—carrier compatibility improves tumour nanotherapy efficacy. *Nat. Commun.* **2016**, *7*, 1–11.
- (46) Wilhelm, S.; Tavares, A. J.; Dai, Q.; Ohta, S.; Audet, J.; Dvorak, H. F.; Chan, W. C. W. Analysis of nanoparticle delivery to tumours. *Nat. Rev. Mater.* **2016**, *1*, 16014.
- (47) Zhu, Z. Effects of amphiphilic diblock copolymer on drug nanoparticle formation and stability. *Biomaterials* **2013**, *34*, 10238–10248.
- (48) Corrigan, A.; Gorski, L.; Hankins, J.; Perucca, R.; Alexander, M. *Infusion Nursing: An Evidence-Based Approach*; Elsevier Health Sciences, 2009.